



Article

Hybrid Modeling of Persistent Shoreline Oil Residues on Abu Ali Island, Saudi Arabia: Extent, Degree, and Remediation Implications

Zachary Nixon ¹, Jacqueline Michel ^{1,*}, Scott Zengel ², Linos Cotsapas ¹, Harold Fravel ², Jennifer Weaver ¹ and Philip Bambach ¹

¹ Research Planning, Inc., Columbia, SC 29201, USA

² Research Planning, Inc., Tallahassee, FL 32303, USA

* Correspondence: jmichel@researchplanning.com

Abstract: Extensive intertidal asphalt pavements and oiled sediment accumulations extend more than 20 km along the northern shoreline of Abu Ali Island, located north of Jubail on the Arabian (Persian) Gulf coast of Saudi Arabia. This shoreline oiling likely originated from two platforms in the Nowruz oil field, which spilled oil from 1983 to 1985; this was one of the largest marine spills in history, with shoreline impacts that were little known. In this study, we used a novel methodology that combined remote sensing analyses with hybrid machine learning–geostatistical modeling of field-collected data to quantify the distribution, extent, and volume of these contaminated sediments to investigate the mechanisms for their persistence and to support the development of remediation plans. After nearly 40 years, approximately 25,000 m³ of contaminated sediments remain, with nearly 50% of these buried underneath clean sediments. The presence of exposed or subsurface carbonate beach rock platforms or ramps clearly influences the ongoing persistence of these asphalt pavements by protecting them from physical energy and sediment mobilization. These rock platforms complicate potential remediation options, with more than 66% of the modeled volume of asphalt pavement estimated to be directly on top of and in contact with carbonate beach rock. The asphalt pavements present persistent ongoing PAH toxicity and continually shed smaller fragments when exposed to wave energy along with localized sheens and liquid oil, presenting a pathway for ongoing chronic exposure of biota.

Keywords: oil spill; beaches; rocky shore; intertidal; contamination; remediation; machine learning; geostatistics



Citation: Nixon, Z.; Michel, J.; Zengel, S.; Cotsapas, L.; Fravel, H.; Weaver, J.; Bambach, P. Hybrid Modeling of Persistent Shoreline Oil Residues on Abu Ali Island, Saudi Arabia: Extent, Degree, and Remediation Implications. *J. Mar. Sci. Eng.* **2023**, *11*, 785. <https://doi.org/10.3390/jmse11040785>

Academic Editor: Kenneth Lee

Received: 1 March 2023

Revised: 31 March 2023

Accepted: 4 April 2023

Published: 5 April 2023



Copyright: © 2023 by the authors. Licensee MDPI, Basel, Switzerland. This article is an open access article distributed under the terms and conditions of the Creative Commons Attribution (CC BY) license (<https://creativecommons.org/licenses/by/4.0/>).

1. Introduction

Extensive intertidal asphalt pavements and oiled sediment residues are present along the intertidal areas of the northern shoreline of Abu Ali Island, located north of Jubail along the Arabian (Persian) Gulf coast of Saudi Arabia (Figure 1). These pavements extend for more than 20 km along the shoreline and have been present for decades, with initial reports of oil stranding onshore along the Saudi Arabian coast in 1983 [1,2], followed by detailed surveys in 1992, one year after the Gulf War oil spills [3,4]. No shoreline cleanup is known to have occurred on Abu Ali Island. Michel et al. [5] concluded that the main potential source of this oil was likely from two platforms in the Nowruz oil field that spilled oil for over two years from 1983 to 1985 during the Iran–Iraq War. It has been shown that these types of pavements negatively affect intertidal fauna in the Arabian Gulf [6,7] and have potential human health risks [8]. The shoreline impacts of this spill, one of the largest marine oil spills in history [9], have not been fully described, and the extent and volume of these pavements are not well-known. Further, the long-term presence of oil pollution along these exposed shorelines nearly 40 years after the incident is unexpected, and the reasons for this multi-decadal persistence are unknown.



Figure 1. Study extent along Abu Ali Island north of Jubail on the Arabian Gulf coast of Saudi Arabia. Inset shows photograph of typical shoreline location with visible asphalt pavement seaward of sand beach.

The study region is arid and characterized by air temperatures averaging 40 °C in summer, with highs up to 51 °C, and averaging 15 °C in winter [10]. Winds over the Arabian Gulf are strongly influenced by the seasonally reversing Arabian monsoons and dominated by the northwesterly summer and winter shamal winds [10–12]. Although the Arabian Gulf is relatively sheltered from wave energy compared with open ocean regions, Abu Ali Island is subject to the highest wave energies in the region [13], with fetches to the north and northwest of up to 250 km. Seasonal wave energy peaks in winter, corresponding with the shamal winds. Tides are semi-diurnal, with a mean neap tidal range of 1.5 m and a spring tidal range close to 2 m [14].

The northern shore of Abu Ali Island is characterized by a moderately steep, medium-grained sand beach face with an average dip angle of 4.3° and an average mean grain size of 0.31 mm [4]. The beach is backed by small, sparsely vegetated foredunes and fronted in several locations by an intertidal to shallow subtidal rock platform or flat covered with sand bars. In a few locations, the intertidal to shallow subtidal rock platforms extend seaward for hundreds of meters. These platforms, which consist primarily of lithified carbonate sediments and were likely formed in situ in the recent geologic past [15,16], often extend landward under the active beach face. Carbonate beach rock platforms are important geological controls on the morphology and morphodynamics of associated sand beaches [17,18] and are also important controls on the ongoing persistence of oiled pavements, as we will demonstrate.

In 2020, an extensive study was undertaken to survey and model the distribution, extent, and volume of contaminated sediments; understand the mechanisms for their persistence; and support the development of a remediation plan. This study used a novel approach, integrating field data and remotely sensed data using a hybrid machine learning–

geostatistical model, which has not previously been applied to the modeling of intertidal contaminated sediments. Our study serves as a companion to the findings of Michel et al. [5], who reported on the forensic and analytical chemistry of samples collected as part of this work. Other objectives included an assessment of the ecological degradation of intertidal communities in the affected areas and the development of target cleanup endpoints, methods, guidelines, and best management practices to reduce ecological impacts during remediation activities. Here, we present the methods and findings of this study, assess the potential causes of the unexpected persistence of this contamination, and suggest remediation alternatives to remove contaminated sediments whilst minimizing damage to sensitive habitats.

2. Materials and Methods

2.1. Remote Sensing Analysis

The asphalt pavements along the Abu Ali shoreline are located on top of and intermingled with exposed carbonate beach rock platforms, which are partially buried and exposed by seasonal and interannual sand beach erosion and depositional cycles. Historical variability in the subaerial exposure of these pavements and platforms is important to understand in order to model the current extents of both contaminated sediments and rock substrates. High-resolution optical remote sensing imagery has been successfully used to map oil pavements in similar contexts [19]. To understand this variability in total extent over time, pavements and platforms were mapped from high-resolution 4-band satellite imagery acquired from the Pléiades-1A, Pléiades-1B, or GeoEye-1 platforms, with panchromatic spatial resolutions of between 0.41 and 0.5 m in 2010, 2014, and 2018. Each image mosaic was precisely georeferenced to field-collected ground control points using a projective transformation and at least 10 ground control points. The root mean square error (RMSE) was below 0.45 m for each image.

After georeferencing, each set of imagery was segmented into discrete polygonal objects using eCognitionTM software, wherein all pixels in each image were clustered into homogeneous groups. The resulting polygonal image segments were manually assigned a numeric classification as either: (1) an apparent oil pavement; (2) an apparent rock platform; or (3) an indeterminate platform or pavement, based upon the color and image segment context. These classified polygons were then merged and the classification values were summed to yield an index describing the frequency and confidence of a pavement or rock platform presence from 2010 to 2018.

2.2. Field Data Collection

The field assessment was conducted from 26 October to 7 November 2020, when daytime low tides were between 0.30 and 0.40 m above the lowest astronomical tide (LAT). USGS Digital Shoreline Analysis System (DSAS) software [20] was used to generate 253 shore-normal transects at 100 m spacing intervals along the shoreline. At each pre-established transect, detailed surface and subsurface oiling observations were recorded at a minimum of three observation locations across-shore. At each observation location, Shoreline Cleanup Assessment Technique (SCAT) terminology [21] was used to describe the extent and degree of surface oiling. The habitat, geomorphology, surface and subsurface substrate conditions, and sediment grain size were also collected for each observation location. Pits at all observation locations were excavated where possible to a depth of 1 m when located at the berm top or at the top of the beach face, and to a 50 cm depth when located lower on the beach face or tidal flats. Additional observation locations were included along the transect line for transects that contained wider intertidal zones or substantial changes in geomorphology and to document heterogeneous oiling conditions or the presence of subsurface oiling. All observation locations were surveyed using real-time kinematic global positioning system (RTK GPS) units to record the x–y coordinates and elevation. Multiple temporary base stations were established via Precise Point Positioning methods to enable

RTK operation during data collection. Absolute vertical and horizontal root mean square (RMS) positional errors were estimated to be less than 10 cm for all positions.

2.3. Modeling Approach

Field data were combined with remotely sensed data using a two-stage modeling approach in order to quantify the thickness and burial depth of oiling at all locations within the project area. This analysis was conducted using a novel hybrid machine learning spatial interpolation modeling approach [22–25] utilizing two stages, wherein an initial non-spatial predictive model was developed using synoptically available predictors and the resulting model errors or residuals were then generated and modeled using geostatistical interpolations. The interpolated residuals were combined with the initial predictions to generate a final prediction. Separate models were constructed using the same input data, methods, and predictive variables for: (1) intertidal surface elevation; (2) the elevation of the carbonate rock layer, if present; (3) the thickness and percent cover of the continuous oil layer, if present; and (4) the thickness of the clean overburden, if present, above a continuous oiling layer.

A series of raster grids was prepared for the predictor variables using a common 1 m by 1 m cell size for the entire model grid. These included: (1) a preliminary digital elevation model (DEM), prepared by manually digitizing the elevation contours from the field survey data and high-resolution satellite imagery and converted to a DEM via the ANUDEM procedure, as implemented in ArcGIS Pro [26]; (2) a numeric index summarizing the frequency of all pavements and platforms identified in historical imagery via remote sensing; (3) the Euclidean distance to the mapped pavement and platforms; and (4) a raster concave hull boundary, enclosing the empirical extent of the observed continuous oiling.

Initial non-spatial modeling was conducted using the R statistical computing language [27] via random forest regression and classification [28], as implemented by the ‘ranger’ library [29]. Hyperparameter selection and final model fitting for the random forest models were carried out using the ‘caret’ library [29,30], using a spatially blocked, 10-fold cross-validation scheme [31], wherein the observations were grouped by transect and the transects were divided into 10 folds. The subsequent geostatistical interpolation of the initial model residuals was performed using the ‘gstat’ library in R [27,32,33]. To account for the strong spatial anisotropy between the across-shore and along-shore dimensions, an anisotropy ratio of 1:30 was selected via cross-validation and used for the subsequent interpolation. Exponential variograms with a fixed anisotropic range of 50 m across-shore by 1500 m along-shore were fitted for each variable of interest. The kriging variance was assessed by a 5-fold cross-validation. These two modeling stages were executed and combined using the ‘GSIF’ library [34]. The variance of the final model predictions for each variable of interest was taken by combining the variance of the random forest model with the variance of the geostatistical model.

All spatial interpolations were conducted using a commonly employed [35–37] local curvilinear coordinate system 80 m wide that was centered on a long-term average of the approximate mean sea level with a resolution of 1 m in the across-shore dimension and 2.5 m in the along-shore dimension. All field sampling data, as well as values of ancillary continuous predictors, were converted to along- and across-shore coordinates for the modeling and interpolation. The modeling results at the analysis grid node locations were back-transformed to geographic coordinates for the mapping and volume estimation.

For each model, a RMSE value and a pseudo- R^2 value indicating the percent of variance explained were generated for both the initial random forest model and the subsequent geostatistical kriging interpolation via cross-validation (spatially blocked 10-fold cross-validation for random forests and 5-fold for geostatistical kriging). Note that no independent validation dataset was used to evaluate the model performance after fitting. Instead, the spatially blocked 5- and 10-fold validation schemes described above were used to generate multiple independent validation data, wherein each fold was a hold-out

consisting of all observations from 10–20% of all transects. These hold-outs were used during training to avoid overfitting the models.

Individual model outputs were combined to group all locations where oil was predicted to be present into categories of contaminated sediment based on the oil type, location/burial status, and substrate. These locations were classified by percent cover as either continuous (>50%) or discontinuous (<50%), by depth as either surface (<5 cm from surface) or subsurface (>5 cm), and as either on sand or on rock (> or <5 cm of depth to underlying carbonate rock platform). The total model-estimated areal extent, volume, and average thickness of intertidal oiled sediments were computed for each of these categories, as well as the volume and average thickness of the clean sediment overburden where relevant.

The final predicted variance of each individual model was a simple sum of the random forest and geostatistical kriging variances. As no formal theory exists as to how to appropriately estimate the final model variances for these types of hybrid machine learning–geostatistical models [24,25], we used a Monte Carlo approach to estimate the uncertainty of these volumes. Each individual predicted variable was randomly perturbed using the predicted variance estimates for that variable and the total model-estimated areal extent, volume, and average thickness of intertidal oiled sediments and clean overburden were estimated, as described above. This process was repeated 500 times and empirical 90% confidence intervals were computed for each value based upon these repeated estimates.

3. Results

Field observations were made at 1434 locations along 253 transects (Figure 2). In total, oiling of any description was observed at 1089 locations (76%). Surface oiling was observed at 565 locations (39%) and subsurface oiling was observed at 397 locations (28%). Both surface and subsurface oiling were observed at 127 locations (9%) and no oiling was observed at 345 locations (24%).

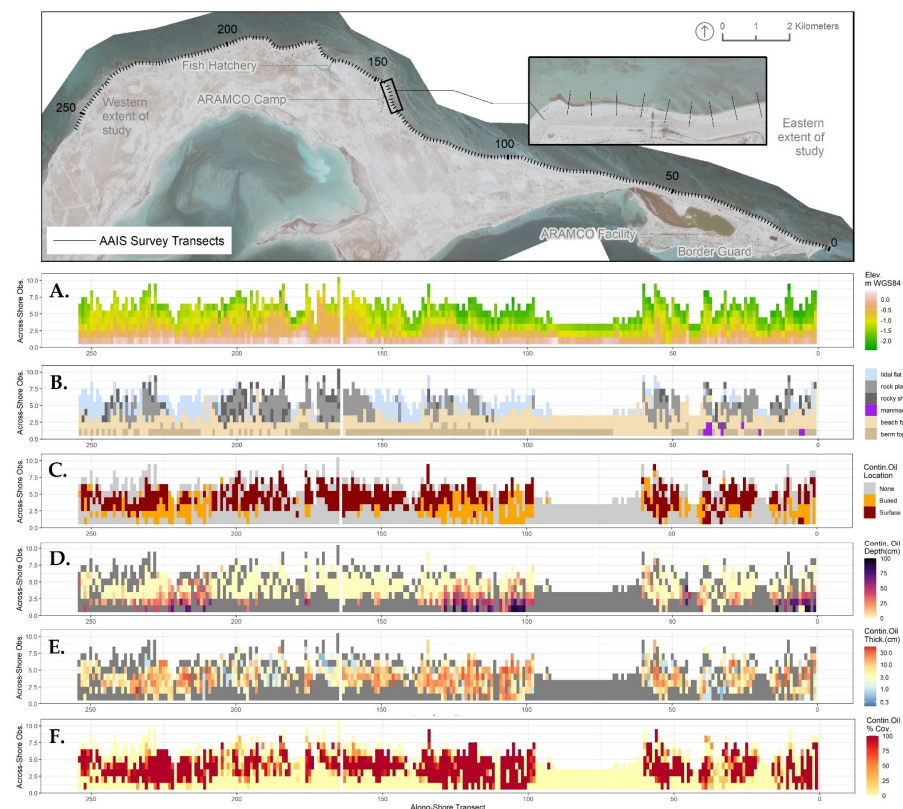


Figure 2. Across-shore tile charts depicting recorded elevation (m WGS84) (A), geomorphology descriptor (B), presence of buried or subsurface oil at each observation location (C), depth of burial of

continuous pavements in cm (D), thickness of continuous pavements in cm (E), and percent cover of continuous pavements at each observation location (F). Each field observation was plotted as a single tile, oriented such that observations made along the same transect appeared as a vertical stack of tiles, with the most landward observation at the bottom and the most seaward observation at the top.

Continuous asphalt pavements or other heavily oiled sediment layers (collectively referred to as pavements hereafter), either buried or exposed at the surface, were the most common type of oil contamination observed during the field assessment (Figure 3). Continuous pavements were observed at 514 observation locations (36%) along 173 unique transects (68%). The thickness of continuous pavements exposed at the surface ranged from <1 cm to 40 cm, with an average thickness of 14 cm. The thickness of continuous pavements buried below the surface ranged from <1 cm to 35 cm, with an average thickness of 12 cm. Small fragments of an oil–sediment mixture, often derived from larger pavements (referred to as tarballs), and other discontinuous oil layers were also commonly observed. Tarballs were observed at 199 of the transects (79%) surveyed. Tarballs were typically found at the surface in the high-tide swash line at the top of the beach face and along the berm top. Tarballs were also commonly found as buried layers within the beach face or in bar features found on sandy tidal flats (Figure 3).

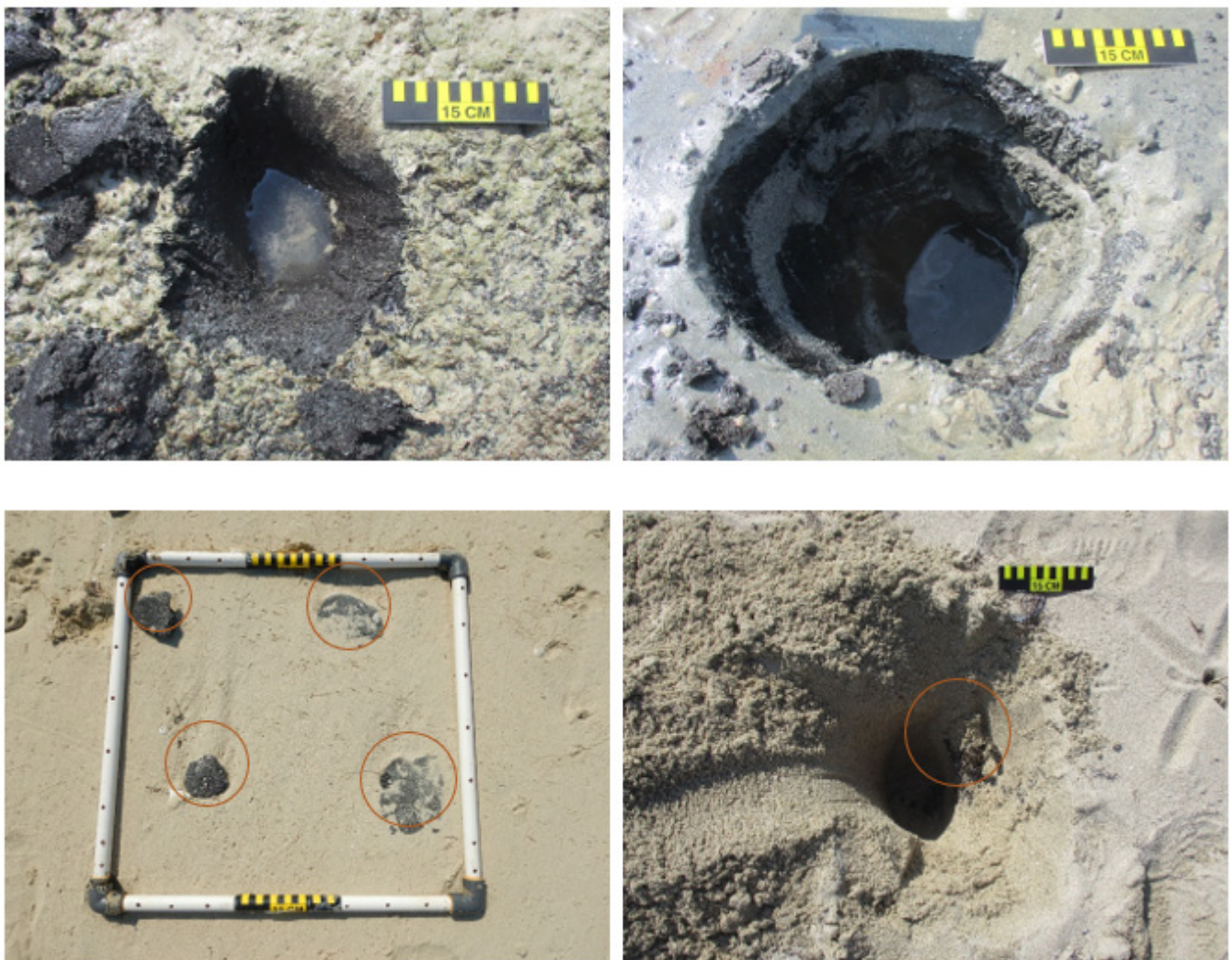


Figure 3. Observed oiling: asphalt pavements exposed at the surface (**top left**) and buried in the subsurface (**top right**); tarballs exposed at the surface (**bottom left**) and buried in the subsurface (**bottom right**). Individual tarballs identified with red circles.

All models performed well (Table 1), with final R^2 values ranging from 86.7% to 99.5%. Predictions of surface and carbonate rock elevation as well as the thickness of the oil layer had the highest accuracy. The hybrid modeling process yielded an estimated volume of 22,000 m³ (90% CI: 19,000–25,000 m³) of continuous pavement over about 22 hectares (ha; 90% CI: 20–23 ha) of the intertidal area along approximately 19.9 km of shoreline or 79% or the evaluated shoreline length (Table 2; Figure 4). An additional 2900 m³ (90% CI: 1500–7500 m³) of discontinuously oiled sediments (tarballs or other sediments with visual oil coverage less than 50%) was estimated to be present over about 8.4 ha (90% CI: 5–18 ha) of the intertidal area along 20.7 km of shoreline. Most of the shoreline with discontinuous oiling also had pavements present, generally buried below a layer of tarballs or further landward or seaward. Discontinuous tarballs were observed along an additional 4.8 km of shoreline with no pavement present. The 90% confidence intervals for the volumes and areas as derived via the Monte Carlo method for individual oil types, locations, and substrate categories were quite wide (Table 2), but uncertainty as to the total area and volume of oiled sediments was generally lower.

Table 1. Cross-validated root mean squared error (RMSE) and pseudo- R^2 , or % of variance explained, for initial random forest model and after subsequent geostatistical kriging interpolation. Estimates derived from spatially blocked, 10-fold cross-validation for random forests and 5-fold for geostatistical kriging.

Modeled Variable	Random Forest Model		Geostatistical Kriging	
	RMSE	R^2	RMSE	R^2
Surface elevation (m)	0.11	96.0%	0.05	99.5%
Thickness of continuous oil layer (cm)	5.6	44.5%	1.0	98.2%
Percent cover of continuous oil layer	25	68.4%	16	86.7%
Thickness of clean overburden (cm)	9.8	71.7%	4.8	93.0%
Elevation of carbonate rock layer (m)	0.14	90.7%	0.08	97.0%

Table 2. Model-estimated areal extent (hectares; ha), volume, and average thickness of intertidal oiled sediments and clean sediment overburden by location (subsurface or surface) and substrate (rock or sand) for continuous and discontinuous oiling. All values reported to two significant digits for volume and area and rounded to nearest whole integer for thickness. Totals may not precisely sum due to rounding in reported values. Empirical 90% confidence intervals derived from Monte Carlo analysis.

Category	Area (ha) (90% CI)	Oiled Sediments		Overburden	
		Volume (m ³) (90% CI)	Average Thickness (cm) (90% CI)	Volume (m ³) (90% CI)	Average Thickness (cm) (90% CI)
Continuous	Surface oiling on sand	2.7 (1.3–4.4)	2200 (1100–3500)	8 (6–10)	-
	Subsurface oiling on sand	6.0 (4.3–7.2)	5300 (3800–6700)	9 (7–11)	17,000 (12,000–20,000)
	Surface oiling on rock	8.2 (5.9–9.6)	9100 (5800–12,000)	11 (10–14)	-
	Subsurface oiling on rock	4.9 (2.7–7.2)	5700 (3000–9200)	12 (10–14)	12,000 (6500–17,000)
	Total Continuous	22 (20–23)	22,000 (19,000–25,000)	-	29,000 (27,000–31,000)

Table 2. Cont.

Category	Area (ha) (90% CI)	Oiled Sediments		Overburden	
		Volume (m ³) (90% CI)	Average Thickness (cm) (90% CI)	Volume (m ³) (90% CI)	Average Thickness (cm) (90% CI)
Discontinuous	Surface oiling on sand	1.6 (0.5–3.4)	490 (130–1300)	3 (2–5)	-
	Subsurface oiling on sand	3.5 (1.0–6.5)	1100 (360–7800)	3 (2–4)	8400 (2000–24,000)
	Surface oiling on rock	2.5 (0.7–7.2)	930 (260–3400)	4 (3–5)	-
	Subsurface oiling on rock	0.8 (0.2–4.2)	320 (80–1700)	4 (3–6)	990 (70–1300)
	Total Discontinuous	8.4 (5–18)	2900 (1500–7500)	-	9500 (4300–31,000)

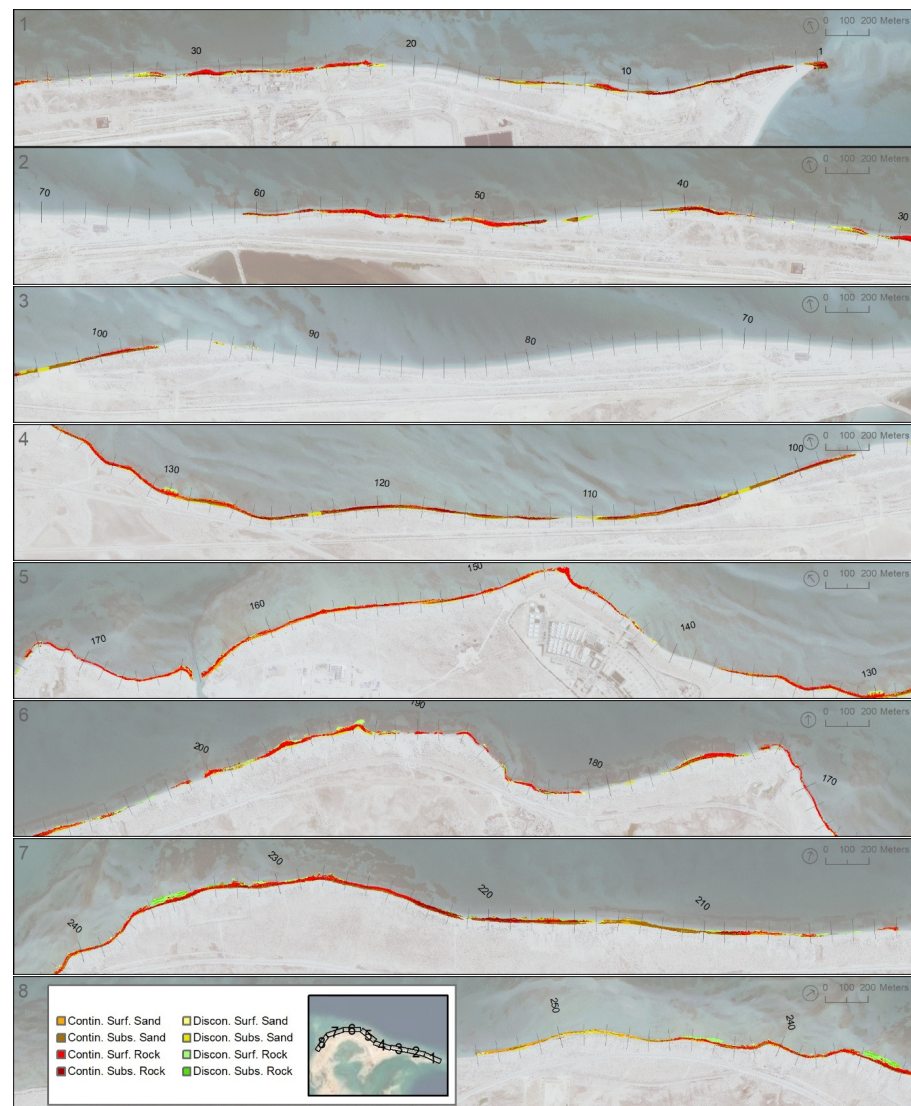


Figure 4. Maps of model-derived intertidal oil location and type categories across the project area. Labels at intervals of 10 transects. Subfigures labeled 1 through 8, sequentially from east to west.

4. Discussion

The continued persistence of such large volumes ($\sim 25,000 \text{ m}^3$) of contaminated sediments on the exposed beaches of the north shore of Abu Ali Island for nearly 40 years is striking. The shoreline is relatively exposed to wave energy, which has generally been correlated with faster rates of oil removal after stranding for other incidents [21,38,39]. This is likely a function of the large volume of oil that was initially stranded. The initial oil loading of this shoreline during the Nowruz spill is unknown because of the elapsed time and lack of available data. The total volume of oil spilled between 1983 and 1985 has been estimated at 1,900,000 barrels or 260,000 tons [9], making this one of the largest known marine oil spills.

The presence of exposed or subsurface carbonate beach rock platforms or ramps clearly influences the ongoing persistence of these oil pavements. More than 66% of the modeled volume of pavement was estimated to be directly on top of and in contact with carbonate beach rock, either buried or exposed at the surface. Of the 54 transects with no observed beach rock, pavements were only observed at 15 transects (39%). We speculated that this was primarily due to the limited sediment mobility of geologically constrained beaches. The morphodynamics of beaches composed of both rock and sediments are relatively poorly studied [40], but reduced beach sediment mobility due to the trapping and wave-sheltering effects of adjacent and underlying rock ramps and platforms has been noted by other researchers [18,41]. It is also possible that reduced hydraulic permeability above the subsurface beach rock platforms may be contributing to the lack of weathering and removal by subsurface beach groundwater flow [42].

The specific effects of the geological control exerted by rock on the persistence of spilled oil on sand beaches has not been previously investigated to our knowledge. Souza et al. [43], in their investigation of a marine mine tailing spill, found that sediments on beaches constrained by carbonate beach rock retained significantly higher concentrations of contaminants than those on a similarly exposed but geologically unconstrained delta plain beach. For oil spills specifically, analogs from other geological settings also occur. Researchers studying oil spills on coarse-grained gravel beaches found that locations in the vicinity of transitions in an along-shore morphology, where a permeable substrate transitions to an impermeable bedrock substrate or where a permeable substrate is sheltered by bedrock tombolos or outcrops, were more likely to harbor long-term subsurface oil from the *Exxon Valdez* oil spill [44,45].

The extensive volume of pavements directly atop or near beach rock platforms and ramps presents a special remediation challenge. Remediation methods applicable for sand beaches are often quite different from those appropriate for rock substrates [21]. Further, substantial populations of living biota are often present on adjacent uncontaminated and exposed rock platforms and ramps. Care must be taken to avoid an unwanted impact on these important ecological areas from mechanical equipment operations, maneuvering, transit, foot traffic, and the stockpiling of materials during remediation.

The persistent continuous pavements were almost certainly the primary source of all tarballs and other discontinuous oiling observed. Biomarker ratios for the samples collected as part of the same field campaign indicated that nearly all oil samples collected were from the same source and were similarly weathered [5]. This implied that the persistent continuous pavements shed smaller fragments when intermittently exposed to wave energy. Similar phenomena were observed in studies on beaches during the *Deepwater Horizon* oil spill, where multiple researchers investigated the long-term generation, transport, burial, and exhumation of sand and oil agglomerates [46–50].

The mean total polycyclic aromatic hydrocarbon (tPAH) concentration in the 44 oil samples collected in 2020 was 418.5 mg/kg [5]. All samples were well above the concentration of tPAH of 90.6 mg/kg that has been determined to pose a high risk to benthic organisms [51], indicating a persistent high degree of ongoing toxicity. The persistence of toxicity in these oil pavements after nearly 40 years was also unexpected. This is likely due to both the thickness of the pavements and their protection from physical processes by the

adjacent rock as well as the inhibition of biodegradation due to extremely high porewater salinity [52]. High regional summer temperatures yield very high surface water salinities, averaging 40 to 45 parts per thousand (ppt) in adjacent open water [53], which then may become hypersaline as beach porewater due to evaporation [54].

Whilst the exterior of these pavements may be more biologically inert, the sediments in the interior remain less weathered and more toxic [55]. The continual generation of tarballs from their parent pavements—whereby more toxic pavement interiors are exposed by mechanical means, also resulting in localized releases of sheen and liquid oil due to high solar irradiance and air temperatures—are pathways for ongoing, chronic exposure of biota in beach, rocky shore, tidal flat, and nearshore habitats. Key beach and tidal flat species identified on the sand substrates included ghost crabs (*Ocyropode rotundata*) and several marine snails (e.g., *Clypeomorus bifasciata persica*, *Mitrella blanda*, and *Nassarius arcularia plicatus*). Intertidal portions of seagrass beds (*Halodule uninervis*) were also located on the sandy tidal flats. For rocky shores, key species included multiple species of marine snails distributed at different tidal elevations (*Echinolittorina arabica*, *Planaxis sulcatus*, *Cerithium caeruleum*, *Clypeomorus bifasciata persica*, *Tylothais savignyi*, *Trochus kotschy*, *Lunella coronata*, and *Monodonta nebulosa*). Heavy surface oiling—primarily, exposed asphalt pavements—was observed to be interfering with the typical key species distributions and abundances on both sandy and rocky shores. Multiple observations of snails with oiling on their shells indicated that residual oiling was still transferable to biota.

Roughly 50% of the modeled volume of continuous oiled sediments and pavements were buried by clean sand. The average depth of this burial was greater than 20 cm, and the resultant modeled volume of clean overburden was greater than the estimated volume of oiled sediments. This poses a substantial remediation challenge for several reasons. First, the continued burial and exhumation of pavements makes physically locating them and identifying their extent challenging. Only 20% of the total area of pavements mapped via the remote sensing analysis was exposed and visible at all three imagery time intervals, implying the continual redistribution of sediments atop oil pavements. Second, the process of side casting the clean overburden, excavating underlying oil pavements, and replacing the clean sediment is more time-consuming and labor-intensive than removing pavements exposed at the surface.

We propose a sediment remediation plan consisting of two phases. Phase I is the excavation of continuous pavement layers, with detailed guidance on the methods and performance endpoints for layers that are over sand and over or attached to rock platforms. A combination of mechanical and manual excavation methods should be used as appropriate based on the extent and depth of the oiled pavement, ecological sensitivity, beach access, and other considerations. Of particular concern is minimizing the excess removal of clean sand and avoiding damage to the rock platforms. The rock platforms stabilize the beaches on Abu Ali Island, and we recommend that they are not fractured, displaced, or excavated. Phase II is the plowing and sifting of all targeted remediation areas (excavated areas treated in Phase I and areas of discontinuous pavement), again with guidance on the methods and performance endpoints for layers that are over sand and over or attached to rock platforms. The goal is to bring the remaining oiled sediments to the surface for removal (by sifting and/or manual methods) and to break up oil residues to speed up the natural degradation. In all phases, detailed best management practices should be put into practice during construction and remediation activities to protect sensitive habitats and biota, including wildlife and fishery resources. Remediation in particularly sensitive areas should be tightly controlled, minimized, or avoided.

5. Conclusions

We estimate that nearly 25,000 m³ of contaminated sediments remain along approximately 76% of the intertidal area along the northern shoreline of Abu Ali Island, persisting for nearly four decades after being stranded during continuous spills from two platforms in the Nowruz oil field from 1983 to 1985. Most of these contaminated sediments persist in

the form of continuous asphalt pavements and nearly 50% of these pavements are buried underneath clean sediments. The presence of exposed or subsurface carbonate beach rock platforms and ramps influences the ongoing persistence of these pavements by protecting them from incident wave energy and complicating potential remediation options. These oil pavements demonstrate persistent ongoing toxicity to benthic organisms, likely due to their thickness and protection from physical energy, as well as a reduction in biodegradation rates due to high porewater salinity. The oil pavements continually shed smaller tarball fragments, sheens, and liquid oil when exposed to wave energy, presenting a pathway for the ongoing chronic exposure of biota.

The successful design of remediation options requires an understanding of both the areas and volumes of contaminated material with quantified uncertainties in categories relevant for the practical application of cleanup techniques. In this study, we used a novel modeling methodology that integrated remote sensing analyses with in situ data using a hybrid machine learning–geostatistical modeling approach to estimate the amount and configuration of contaminated sediments. As researchers in other domains have found, this modeling methodology is more accurate than modeling solely based on spatially explicit covariates or a purely geostatistical approach. Similar modeling methods can be applied as part of investigations into intertidal contamination in other locations from other incidents. In this investigation, we had the luxury of time for the survey planning and analysis, but this is often not true during emergency responses. This analysis framework may be applicable to future responses, where data collected in situ are limited relative to available remotely sensed data. Further, similar approaches could be used to prioritize data collection efforts in areas where field data collection is limited.

Author Contributions: Conceptualization, Z.N., J.M., L.C. and S.Z.; methodology, Z.N.; investigation, J.M., Z.N., L.C., S.Z., H.F., J.W. and P.B.; writing—original draft preparation, Z.N.; illustrations, Z.N., S.Z. and J.M.; writing—review and editing, J.M., Z.N., L.C., S.Z. and J.W. All authors have read and agreed to the published version of the manuscript.

Funding: The field data collection and sample analysis were funded under a contract to Pandion Saudia Company, Ltd. from the National Center for Environmental Compliance, Kingdom of Saudi Arabia. Research Planning, Inc. funded the preparation of the manuscript.

Institutional Review Board Statement: Not applicable.

Informed Consent Statement: Not applicable.

Data Availability Statement: The data presented in this study are available on request from the corresponding author.

Conflicts of Interest: The authors declare no conflict of interest.

References

1. Al-Amirah, A. Oil pollution in the Arabian Gulf: Nowruz oil spill and its impact. A case study of Saudi Arabia. *Geogr. Bull.* **1985**, *37*, 16–32.
2. Fayad, N.M. Identification of tar balls following the Nowruz oil spill. *Mar. Environ. Res.* **1986**, *18*, 155–163. [\[CrossRef\]](#)
3. Hayes, M.O.; Michel, J.; Montello, T.M.; Aurand, D.V.; Al-Mansi, A.M.; Al-Momen, A.H.; Sauer, T.C.; Thayer, G.W. Distribution and weathering of shoreline oil one year after the Gulf War oil spill. *Mar. Pollut. Bull.* **1993**, *27*, 135–142. [\[CrossRef\]](#)
4. Al-Mansi, A.M.; Montello, T.M.; Al-Momen, A.H. Seasonal profile changes in the western Arabian Gulf. In *Marine Wildlife Sanctuary for the Arabian Gulf. Environmental Research and Conservation Following the 1991 Gulf War Oil Spill*; Krupp, F., Abuzinada, A.H., Nader, I.A., Eds.; NCWCD, Riyadh and Senckenberg Research Institute: Frankfurt, Germany, 1996; pp. 33–290.
5. Michel, J.; Nixon, Z.; Cotsapas, L.; Zengel, S.; Weaver, J.; Fravel, H.; Bambach, P. Forensic Analysis of Residual Oil along Abu Ali Island, Saudi Arabia. *J. Mar. Sci. Eng.* **2022**, *10*, 1877. [\[CrossRef\]](#)
6. Giraldes, B.W.; Al-Thani, J.A.K.D.; Dib, S.; Engmann, A.; Alsaadi, H.A.; Vethamony, P.; Alatalo, J.M.; Yigiterhan, O. Target gastropods for standardizing the monitoring of tar mat contamination in the Arabian Gulf. *Reg. Stud. Mar. Sci.* **2022**, *53*, 102328. [\[CrossRef\]](#)
7. Lee, J.; Kim, T.; Yoon, S.O.; Kim, S.; Lee, A.H.; Kwon, B.O.; Allam, A.A.; Al-Khedhairi, A.A.; Lee, H.; Kim, J.J.; et al. Multiple evaluation of the potential toxic effects of sediments and biota collected from an oil-polluted area around Abu Ali Island, Saudi Arabia, Arabian Gulf. *Ecotoxicol. Environ. Saf.* **2019**, *183*, 109547. [\[CrossRef\]](#)

8. Al-Kahtany, K.; El-Sorogy, A.S. Contamination and health risk assessment of the surface sediments along Ras Abu Ali Island, Saudi Arabia. *J. King Saud Univ.—Sci.* **2023**, *35*, 102509. [\[CrossRef\]](#)
9. National Oceanic and Atmospheric Administration (NOAA). *Oil Spill Case Histories*; NOAA/Hazardous Materials Response and Assessment Division: Seattle, WA, USA, 1992.
10. Al Senafi, F.; Anis, A. Shamals and climate variability in the Northern Arabian/Persian Gulf from 1973 to 2012. *Intern. J. Climat.* **2015**, *35*, 4509–4528. [\[CrossRef\]](#)
11. Rao, P.G.; Al-Sulaiti, M.; Al-Mulla, A.H. Winter Shamals in Qatar, Arabian Gulf. *Weather* **2001**, *56*, 444–451. [\[CrossRef\]](#)
12. Yu, Y.; Notaro, M.; Kalashnikova, O.V.; Garay, M.J. Climatology of summer Shamal wind in the Middle East. *J. Geophys. Res. Atmos.* **2016**, *121*, 289–305. [\[CrossRef\]](#)
13. Kamranzad, B.; Etemad-Shahidi, A.; Chegini, V. Assessment of wave energy variation in the Persian Gulf. *Ocean Eng.* **2013**, *70*, 72–80. [\[CrossRef\]](#)
14. Saudi Aramco. *Saudi Aramco Tide Tables, Arabian Gulf, 2020*; Saudi Aramco Environmental Protection Department: Dammam, Saudi Arabia, 2019.
15. Shinn, E.A. Submarine lithification of Holocene carbonate sediments in the Persian Gulf. *Sedimentology* **1969**, *12*, 109–144. [\[CrossRef\]](#)
16. Voudoukas, M.I.; Velegrakis, A.F.; Plomaritis, T.A. Beachrock occurrence, characteristics, formation mechanisms and impacts. *Earth-Sci. Rev.* **2007**, *85*, 23–46. [\[CrossRef\]](#)
17. Jackson, D.W.T.; Cooper, J.A.G.; Del Rio, L. Geological control of beach morphodynamic state. *Mar. Geol.* **2005**, *216*, 297–314. [\[CrossRef\]](#)
18. Gallop, S.L.; Kennedy, D.M.; Loureiro, C.; Naylor, L.A.; Muñoz-Pérez, J.J.; Jackson, D.W.; Fellowes, T.E. Geologically controlled sandy beaches: Their geomorphology, morphodynamics and classification. *Sci. Total Environ.* **2020**, *731*, 139123. [\[CrossRef\]](#) [\[PubMed\]](#)
19. Rajendran, S.; Al-Khayat, J.A.; Veerasingam, S.; Nasir, S.; Vethamony, P.; Sadooni, F.N.; Al-Kuwari, H.A.S. WorldView-3 mapping of Tarmat deposits of the Ras Rakan Island, Northern coast of Qatar: Environmental perspective. *Mar. Pollut. Bull.* **2021**, *163*, 111988. [\[CrossRef\]](#)
20. Himmelstoss, E.A.; Henderson, R.E.; Kratzmann, M.G.; Farris, A.S. *Digital Shoreline Analysis System (DSAS) Version 5.0 User Guide (No. 2018-1179)*; US Geological Survey: Woods Hole, MA, USA, 2018.
21. NOAA (National Oceanic and Atmospheric Administration). *2013 Shoreline Assessment Manual*, 4th ed.; Emergency Response Division, Office of Response and Restoration, National Oceanic and Atmospheric Administration; U.S. Dept. of Commerce: Seattle, WA, USA, 2013; p. 73.
22. Li, J.; Heap, A.D. A review of comparative studies of spatial interpolation methods in environmental sciences: Performance and impact factors. *Ecol. Inform.* **2011**, *6*, 228–241. [\[CrossRef\]](#)
23. Li, J.; Heap, A.D. Spatial interpolation methods applied in the environmental sciences: A review. *Environ. Model. Softw.* **2014**, *53*, 173–189. [\[CrossRef\]](#)
24. Hengl, T.; Heuvelink, G.B.; Kempen, B.; Leenaars, J.G.; Walsh, M.G.; Shepherd, K.D.; Sila, A.; MacMillan, R.A.; Mendes de Jesus, J.; Tamene, L.; et al. Mapping soil properties of Africa at 250 m resolution: Random forests significantly improve current predictions. *PLoS ONE* **2015**, *10*, e0125814. [\[CrossRef\]](#)
25. Hengl, T.; Nussbaum, M.; Wright, M.N.; Heuvelink, G.B.; Gräler, B. Random forest as a generic framework for predictive modeling of spatial and spatio-temporal variables. *PeerJ* **2018**, *6*, e5518. [\[CrossRef\]](#)
26. Hutchinson, M.F.; Xu, T.; Stein, J.A. Recent progress in the ANUDEM elevation gridding procedure. *Geomorphometry* **2011**, *2011*, 19–22.
27. R Core Team. R: A Language and Environment for Statistical Computing. R Foundation for Statistical Computing, Vienna, Austria. Available online: <https://www.R-project.org/> (accessed on 30 March 2023).
28. Breiman, L. Random forests. *Mach. Learn.* **2001**, *45*, 5–32. [\[CrossRef\]](#)
29. Wright, M.N.; Ziegler, A. Ranger: A fast implementation of random forests for high dimensional data in C++ and R. *arXiv* **2015**, arXiv:1508.04409. [\[CrossRef\]](#)
30. Kuhn, M. Caret: Classification and Regression Training. R Package Version 6.0-86. Available online: <https://CRAN.R-project.org/package=caret> (accessed on 30 March 2023).
31. Meyer, H.; Reudenbach, C.; Wöllauer, S.; Nauss, T. Importance of spatial predictor variable selection in machine learning applications—Moving from data reproduction to spatial prediction. *Ecol. Model.* **2019**, *411*, 108815. [\[CrossRef\]](#)
32. Pebesma, E.J. Multivariable geostatistics in S: The gstat package. *Comput. Geosci.* **2004**, *30*, 683–691. [\[CrossRef\]](#)
33. Gräler, B.; Pebesma, E.; Heuvelink, G. Spatio-Temporal Interpolation using gstat. *R J.* **2016**, *8*, 204–218. [\[CrossRef\]](#)
34. Hengl, T. GSIF: Global Soil Information Facilities. R Package Version 0.5-5.1. Available online: <https://CRAN.R-project.org/package=GSIF> (accessed on 30 March 2023).
35. Roelvink, D.; Reniers, A.J.H.M.; Van Dongeren, A.; Van Thiel de Vries, J.; Lescinski, J.; McCall, R. *XBeach Model Description and Manual*; Unesco-IHE Institute for Water Education, Delft and Delft University of Technology: Delft, The Netherlands, 2010.
36. Merwade, V.M.; Maidment, D.R.; Goff, J.A. Anisotropic considerations while interpolating river channel bathymetry. *J. Hydrol.* **2006**, *331*, 731–741. [\[CrossRef\]](#)

37. Legleiter, C.J.; Kyriakidis, P.C. Spatial prediction of river channel topography by kriging. *Earth. Surf. Process. Landf.* **2008**, *33*, 841–867. [\[CrossRef\]](#)
38. Etkin, D.S.; French-McCay, D.; Michel, J. *Review of the State-of-the-Art on Modeling Interactions between Spilled Oil and Shorelines for the Development of Algorithms for Oil Spill Risk Analysis Modeling*; MMS OCS Study 2007-063; Environmental Research Consulting, Cortlandt Manor: New York, NY, USA, 2007; p. 157.
39. Michel, J.; Hayes, M.O.; Brown, P.J. Application of an oil spill vulnerability index to the shoreline of lower Cook Inlet, Alaska. *Envir. Geol.* **1978**, *2*, 107–117. [\[CrossRef\]](#)
40. Trenhaile, A. Rocky coasts—Their role as depositional environments. *Earth-Sci. Rev.* **2016**, *159*, 1–13. [\[CrossRef\]](#)
41. Muñoz-Perez, J.J.; Medina, R. Comparison of long-, medium-and short-term variations of beach profiles with and without submerged geological control. *Coast. Eng.* **2010**, *57*, 241–251. [\[CrossRef\]](#)
42. Li, H.; Boufadel, M.C. Long-term persistence of oil from the Exxon Valdez spill in two-layer beaches. *Natl. Geogr.* **2010**, *3*, 96–99. [\[CrossRef\]](#)
43. Souza, J.R.; Sielski, L.H.; Krause, M.; Souza, B.S.; Brandão, G.P.; Albino, J.; Carneiro, M.T.W.D. The influence of beach geology and morphodynamics on chemical pollution assessments following a mining accident. *Mar. Pollut. Bull.* **2022**, *174*, 113230. [\[CrossRef\]](#) [\[PubMed\]](#)
44. Hayes, M.O.; Michel, J.; Noe, D. Factors controlling initial deposition and long-term fate of spilled oil on gravel beaches. In Proceedings of the 1991 International Oil Spill Conference, San Diego, CA, USA, 4–7 March 1991; pp. 453–460.
45. Nixon, Z.; Michel, J.; Hayes, M.O.; Irvine, G.V.; Short, J. Geomorphic factors related to the persistence of subsurface oil from the Exxon Valdez oil spill. *J. Coastal Res.* **2013**, *69*, 115–127. [\[CrossRef\]](#)
46. Gustitus, S.A.; Clement, T.P. Formation, fate, and impacts of microscopic and macroscopic oil-sediment residues in nearshore marine environments: A critical review. *Rev. Geophys.* **2017**, *55*, 1130–1157. [\[CrossRef\]](#)
47. Dalyander, P.S.; Long, J.W.; Plant, N.G.; Thompson, D.M. Assessing mobility and redistribution patterns of sand and oil agglomerates in the surf zone. *Mar. Pollut. Bull.* **2014**, *80*, 200–209. [\[CrossRef\]](#)
48. Plant, N.G.; Long, J.W.; Dalyander, P.S.; Thompson, D.M.; Raabe, E.A. *Application of a Hydrodynamic and Sediment Transport Model for Guidance of Response Efforts Related to the Deepwater Horizon Oil Spill in the Northern Gulf of Mexico along the Coast of Alabama and Florida (No. 2012-1234)*; US Geological Survey: Reston, VA, USA, 2012.
49. Michel, J.; Owens, E.H.; Zengel, S.; Graham, A.; Nixon, Z.; Allard, T.; Holton, W.; Reimer, P.D.; Lamarche, A.; White, M.; et al. Extent and degree of shoreline oiling: Deepwater Horizon oil spill, Gulf of Mexico, USA. *PLoS ONE* **2013**, *8*, e65087. [\[CrossRef\]](#) [\[PubMed\]](#)
50. Nixon, Z.; Zengel, S.; Baker, M.; Steinhoff, M.; Fricano, G.; Rouhani, S.; Michel, J. Shoreline oiling from the Deepwater Horizon oil spill. *Mar. Pollut. Bull.* **2016**, *107*, 170–178. [\[CrossRef\]](#)
51. Bejarano, A.C.; Michel, J. Large-scale risk assessment of polycyclic aromatic hydrocarbons in shoreline sediments from Saudi Arabia: Environmental legacy after twelve years of the Gulf war oil spill. *Environ. Pollut.* **2010**, *158*, 1561–1569. [\[CrossRef\]](#) [\[PubMed\]](#)
52. Abou Khalil, C.; Fortin, N.; Prince, R.C.; Greer, C.W.; Lee, K.; Boufadel, M.C. Crude oil biodegradation in upper and supratidal seashores. *J. Hazard. Mater.* **2021**, *416*, 125919. [\[CrossRef\]](#)
53. John, V.C.; Coles, S.L.; Abozed, A.I. Seasonal cycles of temperature, salinity and water masses of the western Arabian Gulf. *Oceanol. Acta* **1990**, *13*, 273–281.
54. Geng, X.; Boufadel, M.C.; Jackson, N.L. Evidence of salt accumulation in beach intertidal zone due to evaporation. *Sci. Rep.* **2016**, *6*, 1–5. [\[CrossRef\]](#) [\[PubMed\]](#)
55. Wang, C.; Zhang, Z.; He, S.; Tang, J.; Wang, R.; Liu, X. Environmental fate of polycyclic aromatic hydrocarbons (PAHs) in different layers of tar balls in the Bohai Sea, China. *J. Clean. Prod.* **2023**, *403*, 136803. [\[CrossRef\]](#)

Disclaimer/Publisher’s Note: The statements, opinions and data contained in all publications are solely those of the individual author(s) and contributor(s) and not of MDPI and/or the editor(s). MDPI and/or the editor(s) disclaim responsibility for any injury to people or property resulting from any ideas, methods, instructions or products referred to in the content.